2015-01-1426
Published 04/14/2015
doi:10.4271/2015-01-1426
saetransaf.saejournals.org

Accuracy of SUAS Photogrammetry for Use in Accident Scene Diagramming

Drew A. Jurkofsky
Unmanned Experts

ABSTRACT

Photogrammetry from images captured by terrestrial cameras and manned aircraft has been used for many years to model objects, create scale diagrams and measure distances for use in traffic accident investigation and reconstruction. Due to increasing capability and availability, Unmanned Aircraft Systems (UAS), including small UAS (SUAS), are becoming a valuable, cost effective tool for collecting aerial images for photogrammetric analysis. The metric accuracy of scale accident scene diagrams created from SUAS imagery has yet to be compared to conventional measurement methods, such as total station and laser measurement systems, which are widely used by public safety officials and private consultants.

For this study, two different SUAS were used to collect aerial imagery for photogrammetric processing using PhotoModeler software. A high-resolution consumer grade camera as well as a lower-resolution integrated camera was used as payload to determine the effect of camera resolution on the photogrammetric accuracy of two mock accident scenes. Using a Nikon total station as measurement control, SUAS photogrammetry from both cameras was compared using established targets. As a subjective comparison, the roadway layout was measured without targets and the resultant diagrams were superimposed over the total station control. Results are analyzed and presented in tables and diagrams. The results show the photogrammetric measurement of an accident scene from SUAS aerial imagery provides measurements with errors well below generally accepted ranges for accident reconstruction.

CITATION: Jurkofsky, D., "Accuracy of SUAS Photogrammetry for Use in Accident Scene Diagramming," *SAE Int. J. Trans. Safety* 3(2):2015, doi:10.4271/2015-01-1426.

INTRODUCTION

Traffic accidents are at once tragic, chaotic, frustrating and hazardous locations that present public safety officials with some tremendous challenges: how to safely coordinate rescue efforts, control traffic, forensically document the site and clear the area as quickly as possible, without further injury or death. The rapid spread of capable, cost-effective small Unmanned Aircraft System (SUAS) technology, allied with image processing applications, offer an opportunity to collect forensic-quality scene information, speed up investigations and reduce exposure to hazardous roadside conditions.

Through a cooperative agreement funded by the U.S. Department of Justice' National Institute of Justice, photogrammetry utilizing aerial imagery from SUAS was studied for efficiency and accuracy for use in accident scene measurement and diagramming. While scene efficiency and safety are of great importance to first responders, scene investigators and the public, the current study will focus on the metric accuracy of measurements and scale diagrams created from SUAS imagery.

Photogrammetry from images captured by terrestrial cameras has been used for many years to model objects, create scale diagrams and measure distances for use in traffic accident investigation and reconstruction. The theory and application of terrestrial photogrammetry for accident scene measurements has been well documented by literature [1,2,3,4,5,6,7]. Photogrammetry is used for measurement of roadway evidence such as skid marks, gouges and scratches. It can also be used to determine the placement of vehicles and other items of physical evidence. While some public safety agencies use terrestrial photogrammetry to document accident scenes, it seems the technology is more often used for this purpose during subsequent review by private reconstruction experts. Recently, terrestrial imagery has been used to model vehicle dimensions and measure the depth of crush damage [8,9,10,11,12,13].

Aerial imagery from manned aircraft and satellite imagery is used occasionally for accident scene diagramming and measurement. These images are often used, however, as a backdrop or texture for demonstrative purposes. Fay et al. explained this process using imagery from manned aircraft by which skid marks could be superimposed and three dimensional objects added for realism [14]. Dilich et al. introduced a blimp, or AIRMAP system, outfitted with a 35 mm camera for collecting aerial imagery from an unmanned aircraft. The images could be scaled for analysis or used for demonstrative purposes. The authors noted measurement limitations, such as superelevation and grade, would require terrestrial survey instruments [15]. Finally, aerial imagery for display purposes is a feature common to most accident reconstruction software packages.

Measurement accuracy of accident scenes using terrestrial photogrammetry has been compared to conventional measurement methods by several authors. Using a proprietary software, 3-D

Analytical A, Pepe et al. calculated photogrammetric measurements with an error of less than 12 cm [2]. Tumbas et al. achieved measurement error of about 7.6 cm using a 3-dimensional methodology [3]. A study sponsored by the North Carolina Department of Justice Academy, comparing terrestrial photogrammetric measurement to total station measurement of an accident scene, reported an average error near 1.1 cm over a test range approximately 22 meters wide and 38 meters long [7].

While photogrammetric measurement from terrestrial imagery is well documented and its use for accident reconstruction supported by the literature, less research exists regarding photogrammetric measurement of accident scenes from aerial imagery. This is likely due, in part, to limitations in capturing imagery from manned aircraft, including: expense, geographical limitations and resolution.

The current study of two mock accident scenes will compare photogrammetric measurements from SUAS aerial imagery to those from a total station system. Fixed targets were used to compare the two methods quantitatively while roadway lines and vehicle rest locations were diagrammed and compared qualitatively.

METHOD

Two mock collision scenes were created on a relatively flat asphalt surface with an area approximately 40 meters square. Roadway lines were made with colored tape to create a T-intersection consisting of a main two lane road intersecting with a secondary two lane road. The main road lanes were divided by double yellow lines and had bicycle lanes in each direction. The secondary road lanes were divided by double yellow lines and had no bicycle lanes. A stop sign with a marked stop bar was located on the secondary road where it intersected the main road. Other fixed objects within the scene included two simulated light poles and a fire hydrant.

Circular white plastic targets were used to mark fixed objects and specific physical evidence in each accident scene for a quantitative comparison. The targets were 12 cm in diameter with a small dimple drilled in the center (Figure 1). The targets were fixed to the roadway using double-sided tape so they could not be easily moved. Targets were placed at all four corners of the test area for ground control and subsequent orientation of the photogrammetric measurements (Figure 2). The simulated light poles were placed at the corners of the accident scenes along the main road and were used as two of the ground control points.

An assortment of items, each marked with a comparison target and used to simulate physical evidence, were included in each accident scene. The items were chosen to replicate evidence commonly seen in both accident and crime scenes. Items included a pen, shoes, clothing, handgun, cellphone, keys and coins. An upside down bucket with a circular target on top was added to determine the accuracy of the vertical or z-axis measurement. The purpose of the objects was to add realism to the scene, determine the resolution of individual items from the aerial imagery and add context to the circular targets (Figure 3).

Figure 1. Circular plastic target with a dimple drilled in the center.

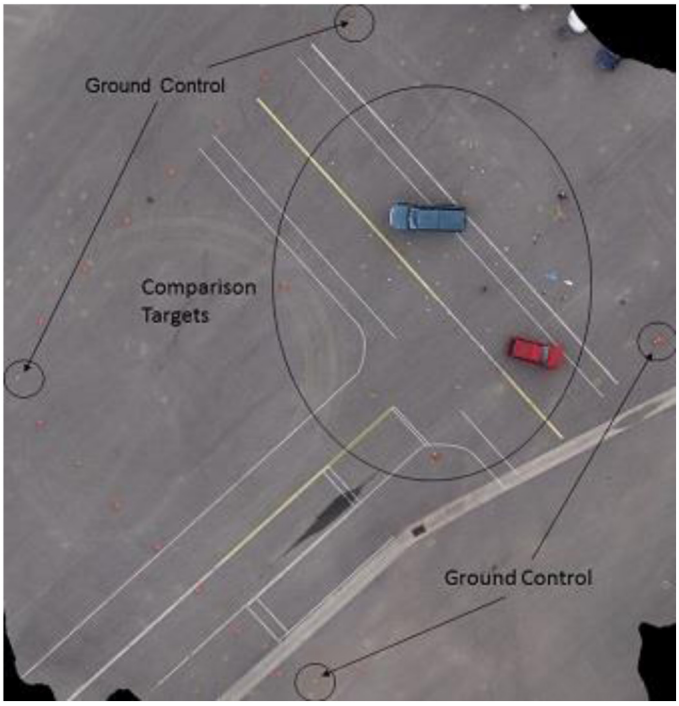

Figure 2. Ground control points were located at the corners of the scene. These total station coordinates were later used to define the coordinate system in PhotoModeler software.

The roadway lines and final rest location for vehicles were measured without specific circular targets for a qualitative comparison. In many cases, investigators may be presented with aerial images that contain no targets or may choose not to apply targets to the roadway layout. Since no targets were specified, the points by which these features were characterized were chosen independently in each method.

Figure 3. Image of a circular plastic target next to a handgun taken by a 24-megapixel camera at 20 meters flying height.

The first mock accident included a Nissan Pathfinder and a Chevrolet Silverado. The accident scenario had the Pathfinder traveling on the primary road and the Silverado traveling on the secondary road. The Silverado stopped at the stop sign, but then completed a left turn in front of the Pathfinder coming from the left of the Silverado. The left front corner of the Pathfinder contacted the left rear corner of the Silverado causing both vehicles to rotate to rest. Skid marks from both vehicles were simulated on the roadway with colored chalk. There were 39 targets placed throughout the scene to mark ground control, physical evidence, the fixed objects and skid marks (Figure 4).

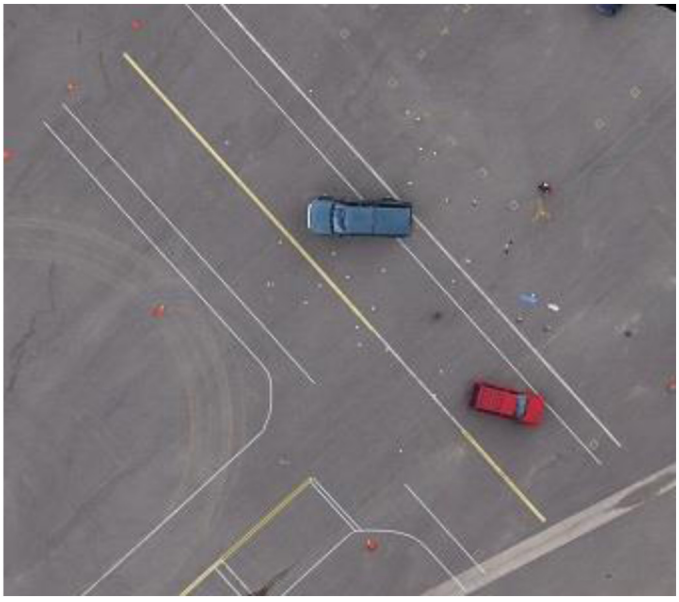

Figure 4. Two vehicle mock accident scene.

The second mock accident was between a Chevrolet Malibu and a bicycle. In the scenario, the Malibu was traveling on the secondary road and disregarded the stop sign at the main road. The bicycle was coming from the right of the sedan and traveling in the bicycle lane closest to the secondary road. The front of the Malibu contacted the left side of the bicycle and threw the bicycle in the direction of the sedan. The Malibu was skidded through the T-intersection to rest so actual skid marks were present. There were 31 targets placed throughout the scene to mark ground control, physical evidence, the fixed objects and skid marks (Figure 5).

Figure 5. Car versus bicycle mock accident scene.

Total Station Measurement

Each mock accident scene was measured with a Nikon NPL-332 pulse laser total station in reflector mode. The instrument measurement setting was precise mode and nine distance measurements were averaged for each point. The total station was about 6 years old, but was recently serviced and calibrated. A mini prism with a 30 mm offset was used as a target on a stabilized prism pole.

Reference measurements were taken with the stabilized prism at the start and end of each measurement session using a steel tape extended about 12 m from directly below the instrument. All of the reference measurements were within ±3 mm of the steel tape measurement, which was within the manufacturer's reported accuracy for the system. Additionally, the reference measurements were well within the measurement uncertainty described by Bartlett et al [16].

For quantitative comparison, measurements were taken with the prism pole tip placed in the center dimple of each circular target. For qualitative comparison, measurements were taken at the ends of each white roadway line and approximately every 10 m between. Double yellow lines were measured similarly except the prism pole was placed in the middle of the yellow lines. Although the same roadway was used for both mock accidents, the lane lines and fixed objects were measured independently for each scene on different days. The position of each vehicle at rest was measured at the center of each wheel and as close as practicable to the vehicle.

Photogrammetric Measurement

Aerial images were collected using two different SUAS. Both UAS airframes were vertical take-off and landing (VTOL) with multiple rotors. Given the multitude of integrated and consumer grade cameras available, all with differing resolutions, the current study used a

low-resolution integrated camera and a high-resolution consumer grade camera. The Aeryon Scout, manufactured by Aeryon Labs, Inc., was powered by 4 rotors (Figure 6). It had an integrated, stabilized camera with a 4-megapixel resolution and 11.9 mm focal length. The DJI S800, manufactured by DJI, was powered by 6 rotors (Figure 7). It was equipped with a Zenmuse brushless gimbal and a Sony NEX-7 24-megapixel camera with a 24mm Zeiss lens.

Figure 6. Aeryon Scout with 4-megapixel integrated, stabilized camera. Manufactured by Aeryon Labs, Inc.

Figure 7. DJI S800 with Zenmuse brushless gimbal and Sony NEX-7 24-megapixel camera with 24 mm Zeiss lens. Manufactured by DJI.

Each flight was planned using the SUAS manufacturer's proprietary mission planning software. The SUAS was flown in a grid pattern over the accident scene while the camera captured highly overlapping nadir images. Image overlap was set at 65% front and back and 55% side to side. The aerial imagery captured by the high-resolution camera for the two vehicle accident scene was collected from a nominal altitude of 30 meters above ground level (AGL). All of the other image sets were collected at a nominal altitude of 20 meters AGL. The average temperature was 27°C with wind speed generally less than 20 km/hr. Flights times were between 8 and 12 minutes. The photogrammetric design criteria for each mock accident scene is summarized in Table 1 and Table 2.

Table 1. Two vehicle accident photogrammetric design criteria.

	Aeryon Scout	DJI S800
Flying Height (m)	20	30
Focal Length (mm)	11.9	24.0
Sensor Size (mm)	9.00 x 6.75	23.5 x 15.6
Image Footprint (m)	15.1 x 11.3	29.4 x 19.5
Number of Images	154	66
Approximate Scale	1:1680	1:1250

Table 2. Car versus bicycle accident photogrammetric design criteria.

	Aeryon Scout	DJI S800
Flying Height (m)	20	20
Focal Length (mm)	11.9	24.0
Sensor Size (mm)	9.00 x 6.75	23.5 x 15.6
Image Footprint (m)	15.1 x 11.3	19.6 x 13.0
Number of Images	91	80
Approximate Scale	1:1680	1:833

PhotoModeler Scanner software, which has been shown accurate for accident reconstruction purposes, was chosen for photogrammetric analysis [5,9,10,11,12,13]. Both cameras were calibrated with PhotoModeler's procedures using coded targets to calculate and correct for lens distortion. Images were processed in PhotoModeler as a SmartMatch project. PhotoModeler referenced SmartMatch points in at least 3 different images and SmartMatch points with a residual greater than 1 pixel were removed from the project. Circular targets, roadway lines and vehicles were manually marked in every image they appeared. Each target was marked in at least 3 images.

For quantitative comparison, the photogrammetric project was oriented and scaled using total station measurements of the ground control corner targets. The ground control points were assigned x, y and z coordinates in PhotoModeler relative to an origin directly under the total station.

In a comparison table, the remaining total station target measurements were compared to the corresponding photogrammetric points. These total station points were not assigned to the photogrammetric points allowing the coordinate measurements for each target to be compared. The 3-dimensional distance between the points measured by total station and photogrammetrically was calculated using the equation:

$$\boldsymbol{3D\ distance} = \sqrt{(x_1 - x_2)^2 + (y_1 - y_2)^2 + (z_1 - z_2)^2} \quad \textit{(EQ.1)}$$

Where x_1, y_1, z_1 = total station point coordinate

x_2, y_2, z_2 = photogrammetric point coordinate

These distances represent the error between the total station point locations and the photogrammetrically calculated points. The circular target errors for each accident scene were averaged to determine the average difference between the coordinate total station measurements and coordinate photogrammetric measurements.

For qualitative comparison, plastic circular markers were placed in the scene before each SUAS flight (Figure 8). The circular markers were 9 cm in diameter and were not measured by total station.

Similar to circular stickers being applied to a vehicle to measure crush damage, the circular markers were used as a reference along curves and long lines so the same point could be easily located in each image. The markers on each line, along with the line ends, were used to photogrammetrically measure the lane lines. Unlike the total station measurement, each individual yellow line was measured instead of estimating the middle.

Figure 8. Circular markers used to reference along a curve.

To measure the vehicle rest locations, markers were placed next to the vehicle wheels and centered at the hub (Figure 9). This was done for each flight mission except for the aerial imagery from the Aeryon Scout of the two vehicle accident.

Figure 9. Circular markers used to mark vehicle rest location.

A total of four scale diagrams were created, one for each camera and from each accident scene, using the oriented photogrammetric measurement point data. The photogrammetric scale diagrams were layered over scale diagrams using the total station measurement point data from each accident scene. Each accident scene diagram with combined measurement data was used for subjective comparison.

RESULTS

The difference in the coordinate total station measurement and coordinate photogrammetric measurement for each circular target was calculated and reported as a distance error. In Appendix A, Tables A1 and A2 show the coordinate data for the two vehicle accident and Tables A3 and A4 show the coordinate data for the car versus bicycle accident. All of the coordinate data was measured in feet and converted to centimeters.

The target distance errors were averaged for each accident scene. Table 3 shows the average error, standard deviation and confidence interval for the two vehicle accident with Table 4 showing the vertical error and standard deviation. Table 5 and Table 6 show the same statistics for the car versus bicycle accident.

Table 3. Two vehicle accident distance error statistics.

	Aeryon Scout	DJI S800
Average Error (cm)	1.20	1.22
Standard Deviation (cm)	0.44	0.25
95% CI (cm)	[1.05,1.34]	[1.14,1.30]
Minimum Error (cm)	0.33	0.67
Maximum Error (cm)	2.01	1.85
Count	35	35

Table 4. Two vehicle accident vertical distance error statistics.

	Aeryon Scout	DJI S800
Average Vertical Error (cm)	-0.98	0.92
Standard Deviation (cm)	0.53	0.34
Minimum Error (cm)	0.00	0.24
Maximum Error (cm)	1.98	1.79

Table 5. Car versus bicycle accident distance error statistics.

	Aeryon Scout	DJI S800
Average Error (cm)	0.66	0.82
Standard Deviation (cm)	0.31	0.27
95% CI (cm)	[0.54,0.78]	[0.72,0.93]
Minimum Error (cm)	0.12	0.27
Maximum Error (cm)	1.40	1.21
Count	27	27

Table 6. Car versus bicycle accident vertical distance error statistics.

	Aeryon Scout	DJI S800
Average Vertical Error (cm)	-0.49	0.60
Standard Deviation (cm)	0.28	0.34
Minimum Error (cm)	0.03	0.03
Maximum Error (cm)	0.94	1.18

The scale diagrams with photogrammetric measurement data layered over the total station measurement data are located in Appendix B for visual comparison. Figures B1 and B2 are diagrams from the two vehicle accident. Figures B3 and B4 are diagrams from the car versus bicycle accident.

DISCUSSION

Quantitative examination of the PhotoModeler measurement data from the high-resolution and low-resolution aerial imagery showed strong agreement with the total station measurement data. All of the photogrammetric measurement sets had a maximum distance error of less than 2 cm with an average distance error between 0.66 and 1.22 cm. These measurements are appropriate for use in accident investigation and reconstruction and are less than errors previously published [2,3,4,5,7].

The distance error along the vertical axis was the greatest overall with an average error between 0.49 and 0.98 cm. The vertical distance error for the target on the bucket (labeled Blk Bucket in Tables A1 and A2 and Hydrant in Tables A3 and A4) was between 0.03 and 1.28 cm with an average of 0.73 cm. Given the target on the bucket was about 37 cm above the roadway surface, it seems reasonable to conclude that photogrammetric measurements can be used on roadways with grade and superelevation. The distance error along the vertical axis, including ways to minimize it, could be explored further in a future study.

The two vehicle accident had imagery captured at 20 meters AGL by the low-resolution camera and 30 meters AGL by the high-resolution camera. The car versus bicycle collision had imagery captured at 20 meters AGL by both cameras. The average error for the low-resolution camera compared to the high-resolution camera showed no significant difference to either accident scene. This was likely due to the circular targets that were used for the aerial imagery. Even though the resolution of the circular targets changed, it was still possible to recognize the circle in each image and place a point in the middle for photogrammetric calculation. Surprisingly, the average distance error from the low-resolution camera was slightly better than the high-resolution camera for both accident scenes.

While the use of circular targets and markers is not required for photogrammetric measurement, their use makes manual point marking on individual images easier. If point marking relied entirely on features within the scene, image resolution would likely affect the accuracy of point placement in each image and thus affect the accuracy of the photogrammetric measurement data. An example of this was the wheel placement for the two vehicle accident that had aerial imagery collected with the low-resolution camera and without circular markers. The greatest distance between the photogrammetric measurement and total station measurement can be seen at the right rear tire of the Pathfinder as shown in Figure 10.

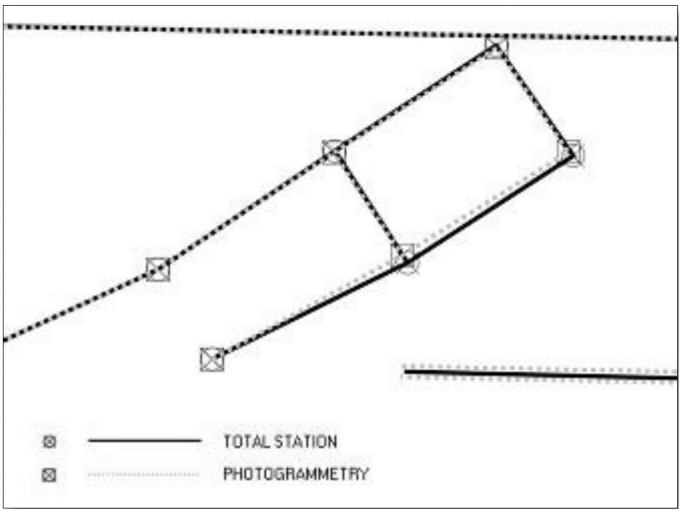

Figure 10. Tire placement error between total station measurements and photogrammetric measurements without circular markers.

The diagrams shown in Figure B1, B2, B3 and B4 allow for qualitative comparison of how well the photogrammetric measurement data fit the total station measurement data for the roadway layout and vehicle wheel placement. The roadway lines in all four diagrams were virtually the same. In general, the photogrammetric wheel placement aligned well with the total station wheel placement for the aerial imagery utilizing circular markers.

The photogrammetric measurement of the Malibu right front wheel, from the bicycle accident with the high-resolution camera, could not be calculated (Figure 11). Two sequential aerial images were out of focus, leaving only one image for marking. Since the wheel marker was only visible in one image, PhotoModeler could not solve for the point location as a point must appear in at least two images to solve for its position. This is a limitation of photogrammetry and a good reason to check all images while still at the scene.

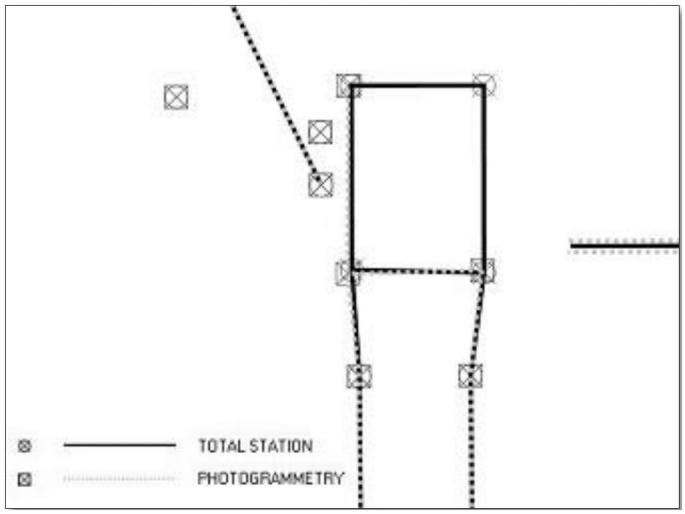

Figure 11. Note the missing photogrammetric measurement for the right front tire.

Photogrammetry from SUAS aerial imagery is a viable alternative to total station measurements with ground control established for scale. Ground control can be established with total station, as shown in the current study, or simply by having a known distance visible in the images. Photogrammetry is useful as it preserves the accident scene in imagery which can be accessed and reviewed at any time. This enables reconstruction experts to independently verify measurements or take additional measurements of the scene.

Photogrammetric software allows for the creation of orthophotos where all of the individual images are stitched together to make a single orthomosaic. Like an aerial image from a manned aircraft, this can be used as a texture for a 3-dimensional model or for demonstrative purposes. Orthophotos from both mock accident scenes are shown in Appendix C. Orthophotos from the two vehicle accident are shown in Figures C1 and C2. Orthophotos from the car versus bicycle accident are shown in Figures C3 and C4.

SUAS aerial imagery does have limitations, primarily related to environmental conditions. The ability for SUAS to operate in high wind, extreme cold, rain and snow is largely dependent on the

individual aircraft. While retro-reflective targets could theoretically be used, aerial photogrammetry generally does not work at night without significant terrestrial lighting. Large tree canopies, overpasses and any other visual obstruction from altitude will also limit the application of this technology. Future studies may want to explore modified flight patterns or payloads to address these limitations.

SUMMARY/CONCLUSIONS

1. The photogrammetric measurement of an accident scene from SUAS aerial imagery provides measurements with errors well below generally accepted ranges for accident reconstruction.
2. The photogrammetric measurement errors from SUAS aerial imagery are consistent with those found in published studies using terrestrial imagery for photogrammetric measurement.
3. Camera resolution, for images captured at 20 meters AGL or between images captured at 20 meters AGL from a low-resolution camera and 30 meters AGL from a high-resolution camera, does not affect photogrammetric accuracy when circular targets are used for reference. However, photogrammetric accuracy may be affected by camera resolution when targets are not used.
4. With the exception of environmental conditions limiting its use, SUAS photogrammetry is a viable alternative to total station measurement when proper ground control is established.

REFERENCES

1. Pepe, M., Sobek, J., and Huett, G., "Three-Dimensional Computerized Photogrammetry and its Application to Accident Reconstruction," SAE Technical Paper 890739, 1989, doi:10.4271/890739.
2. Pepe, M., Sobek, J., and Zimmerman, D., "Accuracy of Three-Dimensional Photogrammetry as Established by Controlled Field Tests," SAE Technical Paper 930662, 1993, doi:10.4271/930662.
3. Tumbas, N., Kinney, J., and Smith, G., "Photogrammetry and Accident Reconstruction: Experimental Results," SAE Technical Paper 940925, 1994, doi:10.4271/940925.
4. Pepe, M., Grayson, E., McClary, A., "Digital Rectification of Reconstruction Photographs," SAE Technical Paper 961049, 1996, doi:10.4271/961049.
5. Fenton, S. and Kerr, R., "Accident Scene Diagramming Using New Photogrammetric Technique," SAE Technical Paper 970944, 1997, doi:10.4271/970944.
6. Cooner, S., and Balke, K., "Use of Photogrammetry for Investigation of Traffic Incident Scenes," Texas Transportation Institute, Report No. TX-99/4907-2, October 2000.
7. iWitness Close Range Photogrammetry, "Accuracy Performance of the Close-Range Photogrammetry System iWitness: Results of a Measurement Comparison with a Surveying Total Station," http://www.iwitnessphoto.com/iwitness/accuracy_study3.html, accessed Oct. 2014.
8. Breen, K. and Anderson, C., "The Application of Photogrammetry to Accident Reconstruction," SAE Technical Paper 861422, 1986, doi:10.4271/861422.
9. Fenton, S., Johnson, W., LaRocque, J., Rose, N., et al., "Using Digital Photogrammetry to Determine Vehicle Crush and Equivalent Barrier Speed (EBS)," SAE Technical Paper 1999-01-0439, 1999, doi:10.4271/1999-01-0439.
10. Switzer, D., and Candrlic, T., "Factors affecting the accuracy of Non-Metric Analytical 3-D Photogrammetry, Using PhotoModeler," SAE Technical Paper 1999-01-0451, 1999, doi:10.4271/1999-01-0451.
11. O'Shields, L., Kress, T., Hungerford, J., and Aikens, C., "Determination and Verification of Equivalent Barrier Speeds (EBS) Using PhotoModeler as a Measurement Tool," SAE Technical Paper 2004-01-1208, 2004, doi:10.4271/2004-01-1208.
12. Mills, D., and Carty, G., "Semi-Automated Crush Determination Using Coded and Non-Coded Targets with Close-Range Photogrammetry," http://www.photomodeler.com/applications/documents/MillsCodedTargetsCrush.pdf, accessed Oct. 2014.
13. Randles, B., Jones, B., Welcher, J., Szabo, T., et al., "The Accuracy of Photogrammetry vs. Hand-on Measurement Techniques used in Accident Reconstrucion," SAE Technical Paper 2010-01-0065, 2010, doi:10.4271/2010-01-0065.
14. Fay, R., Robinette, R., and Larson, V., "Engineering Models and Animations in Vehicular Accident Studies," SAE Technical Paper 880719, 1988, doi:10.4271/880719.
15. Dilich, M., and Goebelbecker, J., "Accident Investigation and Reconstruction Mapping with Aerial Photography," SAE Technical Paper 960894, 1996, doi:10.4271/960894.
16. Bartlett, W., Wright, W., Masory, O., Brach, R. et al., "Evaluating the Uncertainty in Various Measurement Tasks Common to Accident Reconstruction," SAE Technical Paper 2002-01-0546, 2002, doi:10.4271/2002-01-0546.

CONTACT INFORMATION

Drew A. Jurkofsky
Unmanned Experts
720 S. Colorado Boulevard
Penthouse North
Denver, CO 80246
drew.j@unmannedexperts.com

ACKNOWLEDGMENTS

The author would like to acknowledge the assistance of David Prall and Edwin Freeborn of Unmanned Experts whose participation and input was invaluable to this study, and technical assistance provided by PhotoModeler, developed by Eos Systems, Inc. Additionally, the comparison of two SUAS with different cameras would not have been possible without the assistance of Aeryon Labs, Inc., which generously loaned the Aeryon Scout for use in this study.

This project was supported by Award No. 2013-IJ-CX-K008, awarded by the National Institute of Justice, Office of Justice Programs, U.S. Department of Justice. The opinions, findings, and conclusions or recommendations expressed in this document are those of the author and do not necessarily reflect those of the Department of Justice.

APPENDIX

APPENDIX A: MEASUREMENT DATA

MOCK ACCIDENT SCENE 1: TWO VEHICLE ACCIDENT

Table A1. PhotoModeler (PM) and total station (TS) coordinate point measurement data using a 4-megapixel camera at 20 meters flying height.

Scout	PM X	PM Y	PM Z	TS X	TS Y	TS Z	DX	DY	DZ	Ave Error
Back Skid 1	-16.814	-24.022	0.000	-16.839	-24.020	0.043	0.026	-0.003	-0.043	0.050
Back Skid 2	-12.439	-29.070	-0.074	-12.452	-29.075	-0.027	0.013	0.005	-0.047	0.049
Back Skid 3	-8.547	-35.415	-0.162	-8.556	-35.415	-0.111	0.009	0.000	-0.051	0.052
Back Skid 4	-5.286	-41.947	-0.252	-5.295	-41.955	-0.200	0.009	0.007	-0.051	0.052
Blk Bucket	0.786	-27.597	0.959	0.791	-27.592	0.988	-0.006	-0.005	-0.029	0.030
Blue Ring	-21.115	-14.201	0.110	-21.130	-14.227	0.143	0.014	0.027	-0.033	0.045
Cable	-1.917	-20.828	-0.114	-1.909	-20.843	-0.093	-0.008	0.014	-0.021	0.026
Cellphone	-2.871	-16.196	-0.080	-2.877	-16.204	-0.061	0.005	0.009	-0.019	0.021
Coins	-25.310	-46.766	-0.088	-25.290	-46.786	-0.043	-0.019	0.020	-0.045	0.053
Front Skid 1	-25.088	-32.509	0.036	-25.120	-32.507	0.086	0.032	-0.002	-0.051	0.060
Front Skid 2	-21.164	-33.794	-0.002	-21.182	-33.790	0.053	0.019	-0.004	-0.055	0.058
Front Skid 3	-16.137	-34.907	-0.084	-16.156	-34.919	-0.033	0.019	0.012	-0.051	0.056
Gloves	0.005	-8.953	-0.057	0.000	-8.965	-0.049	0.005	0.012	-0.008	0.016
Gun	-10.236	-7.723	0.034	-10.250	-7.737	0.041	0.013	0.014	-0.007	0.021
Hydrant	-35.739	-64.451	-0.071	-35.733	-64.459	-0.006	-0.006	0.008	-0.065	0.066
Jeans	10.225	-11.697	-0.189	10.234	-11.717	-0.189	-0.009	0.020	0.000	0.022
Keys	-46.671	-16.061	0.352	-46.688	-16.068	0.387	0.016	0.007	-0.035	0.040
Knife	-18.031	-44.037	-0.124	-18.019	-44.050	-0.085	-0.013	0.013	-0.039	0.043
L Shoe	11.765	-16.520	-0.239	11.767	-16.541	-0.236	-0.001	0.021	-0.003	0.022
L Skid 1	8.996	-34.183	-0.374	8.986	-34.188	-0.350	0.010	0.005	-0.024	0.027
L Skid 2	-0.992	-38.789	-0.277	-1.003	-38.795	-0.236	0.011	0.006	-0.041	0.043
L Skid 3	-7.983	-40.055	-0.205	-7.999	-40.059	-0.153	0.016	0.004	-0.052	0.055
L Skid 4	-18.531	-39.840	-0.074	-18.541	-39.850	-0.037	0.010	0.010	-0.037	0.040
L Skid 5	-29.650	-39.739	-0.023	-29.661	-39.735	0.019	0.011	-0.004	-0.041	0.043
Org Cap	-50.220	-34.197	0.317	-50.239	-34.200	0.376	0.019	0.002	-0.059	0.062
Paint Brush	-24.453	-8.295	0.217	-24.478	-8.316	0.250	0.025	0.021	-0.034	0.047
Pen	-28.939	-4.803	0.241	-28.960	-4.821	0.260	0.021	0.019	-0.019	0.034
Purple Ring	-22.026	-6.946	0.187	-22.049	-6.965	0.216	0.022	0.019	-0.029	0.041
R Shoe	16.622	-13.737	-0.297	16.633	-13.755	-0.295	-0.012	0.018	-0.002	0.022
R Skid	11.379	-38.191	-0.447	11.387	-38.177	-0.415	-0.008	-0.014	-0.032	0.035
Rock	-31.285	-5.439	0.259	-31.310	-5.452	0.279	0.025	0.013	-0.020	0.035
Shirt	14.242	-9.992	-0.239	14.238	-9.999	-0.232	0.004	0.007	-0.007	0.011
Shoe	-13.968	-11.248	0.034	-13.971	-11.259	0.053	0.003	0.011	-0.019	0.022
Stop Sign	23.289	-66.168	-0.837	23.321	-66.156	-0.800	-0.033	-0.012	-0.036	0.050
Survey Pin	14.827	-50.034	-0.619	14.850	-50.029	-0.598	-0.022	-0.004	-0.021	0.031
					Ave error in feet		0.006	0.008	-0.032	0.039
					Ave error in centimeters		0.193	0.243	-0.982	1.201

Table A2. Raw PhotoModeler (PM) and total station (TS) coordinate point measurement data using a 24-megapixel camera at 30 meters flying height.

DJI S800	PM X	PM Y	PM Z	TS X	TS Y	TS Z	DX	DY	DZ	Ave Error
Back Skid 1	-16.821	-24.011	0.093	-16.839	-24.020	0.043	0.018	0.008	0.050	0.054
Back Skid 2	-12.447	-29.057	0.015	-12.452	-29.075	-0.027	0.005	0.018	0.042	0.046
Back Skid 3	-8.549	-35.406	-0.075	-8.556	-35.415	-0.111	0.007	0.008	0.037	0.038
Back Skid 4	-5.291	-41.943	-0.168	-5.295	-41.955	-0.200	0.004	0.012	0.032	0.034
Blk Bucket	0.778	-27.592	1.030	0.791	-27.592	0.988	-0.013	0.000	0.042	0.044
Blue Ring	-21.123	-14.186	0.178	-21.130	-14.227	0.143	0.006	0.042	0.035	0.055
Cable	-1.930	-20.819	-0.078	-1.909	-20.843	-0.093	-0.021	0.023	0.015	0.034
Cellphone	-2.879	-16.180	-0.035	-2.877	-16.204	-0.061	-0.003	0.024	0.027	0.036
Coins	-25.310	-46.763	-0.003	-25.290	-46.786	-0.043	-0.019	0.023	0.039	0.050
Front Skid 1	-25.100	-32.497	0.118	-25.120	-32.507	0.086	0.020	0.010	0.032	0.039
Front Skid 2	-21.169	-33.789	0.079	-21.182	-33.790	0.053	0.013	0.001	0.025	0.029
Front Skid 3	-16.143	-34.899	-0.010	-16.156	-34.919	-0.033	0.013	0.020	0.023	0.033
Gloves	-0.009	-8.942	-0.031	0.000	-8.965	-0.049	-0.009	0.023	0.018	0.031
Gun	-10.250	-7.710	0.071	-10.250	-7.737	0.041	0.000	0.027	0.030	0.041
Hydrant	-35.742	-64.448	0.053	-35.733	-64.459	-0.006	-0.009	0.011	0.059	0.061
Jeans	10.208	-11.688	-0.173	10.234	-11.717	-0.189	-0.026	0.029	0.016	0.042
Keys	-46.672	-16.052	0.417	-46.688	-16.068	0.387	0.016	0.017	0.029	0.037
Knife	-18.035	-44.032	-0.049	-18.019	-44.050	-0.085	-0.017	0.018	0.036	0.043
L Shoe	11.759	-16.519	-0.213	11.767	-16.541	-0.236	-0.008	0.022	0.023	0.033
L Skid 1	8.988	-34.176	-0.318	8.986	-34.188	-0.350	0.002	0.012	0.032	0.034
L Skid 2	-0.999	-38.784	-0.217	-1.003	-38.795	-0.236	0.004	0.011	0.019	0.022
L Skid 3	-7.988	-40.051	-0.122	-7.999	-40.059	-0.153	0.011	0.008	0.031	0.034
L Skid 4	-18.534	-39.831	0.002	-18.541	-39.850	-0.037	0.007	0.019	0.038	0.044
L Skid 5	-29.650	-39.732	0.055	-29.661	-39.735	0.019	0.011	0.003	0.036	0.038
Org Cap	-50.217	-34.191	0.406	-50.239	-34.200	0.376	0.021	0.009	0.031	0.038
Paint Brush	-24.461	-8.281	0.278	-24.478	-8.316	0.250	0.017	0.035	0.028	0.048
Pen	-28.946	-4.795	0.297	-28.960	-4.821	0.260	0.015	0.026	0.037	0.047
Purple Ring	-22.039	-6.934	0.247	-22.049	-6.965	0.216	0.009	0.030	0.031	0.044
R Shoe	16.610	-13.727	-0.285	16.633	-13.755	-0.295	-0.023	0.028	0.010	0.038
R Skid	11.385	-38.175	-0.366	11.387	-38.177	-0.415	-0.002	0.002	0.049	0.049
Rock	-31.294	-5.428	0.306	-31.310	-5.452	0.279	0.016	0.025	0.027	0.040
Shirt	14.222	-9.981	-0.219	14.238	-9.999	-0.232	-0.016	0.017	0.013	0.027
Shoe	-13.978	-11.235	0.085	-13.971	-11.259	0.053	-0.007	0.024	0.032	0.041
Stop Sign	23.288	-66.165	-0.793	23.321	-66.156	-0.800	-0.034	-0.009	0.008	0.036
Survey Pin	14.818	-50.027	-0.563	14.850	-50.029	-0.598	-0.031	0.002	0.035	0.047
					Ave error in feet		-0.001	0.017	0.030	0.040
					Ave error in centimeters		-0.017	0.506	0.929	1.225

MOCK ACCIDENT SCENE 2: CAR VERSUS BICYCLE ACCIDENT

Table A3. PhotoModeler (PM) and total station (TS) coordinate point measurement data using a 4-megapixel camera at 20 meters flying height.

Scout	PM X	PM Y	PM Z	TS X	TS Y	TS Z	DX	DY	DZ	Ave Error
Bicycle	-19.011	15.059	-0.332	-19.012	15.062	-0.304	0.000	-0.004	-0.028	0.029
Blood	-23.773	8.747	-0.352	-23.765	8.747	-0.336	-0.009	0.000	-0.016	0.018
Cellphone	-23.441	34.521	-0.531	-23.440	34.522	-0.521	-0.001	-0.001	-0.011	0.011
Glove	-22.102	15.582	-0.362	-22.106	15.585	-0.342	0.005	-0.002	-0.020	0.020
Hair Tie	-31.654	55.252	-0.823	-31.662	55.246	-0.802	0.008	0.006	-0.022	0.024
Helmet	-19.440	8.371	-0.257	-19.437	8.372	-0.259	-0.004	-0.002	0.001	0.004
Hydrant	17.042	63.617	0.933	17.011	63.607	0.934	0.031	0.010	-0.001	0.033
Jeans	-27.699	13.269	-0.406	-27.706	13.257	-0.403	0.007	0.012	-0.003	0.015
Knife	-28.558	24.547	-0.503	-28.561	24.557	-0.489	0.004	-0.010	-0.014	0.018
L1	-30.737	47.467	-0.743	-30.761	47.442	-0.712	0.023	0.025	-0.031	0.046
L2	-30.100	59.108	-0.845	-30.118	59.102	-0.821	0.018	0.006	-0.024	0.031
L3	-29.368	75.076	-0.953	-29.391	75.066	-0.935	0.022	0.010	-0.018	0.030
L4	-28.965	85.036	-1.007	-28.984	85.027	-0.988	0.019	0.010	-0.019	0.028
Pen	-35.020	25.657	-0.579	-35.025	25.665	-0.568	0.004	-0.008	-0.011	0.014
Plastic	-29.723	36.500	-0.617	-29.730	36.501	-0.601	0.007	-0.001	-0.016	0.018
R1	-35.691	47.733	-0.820	-35.693	47.732	-0.808	0.002	0.001	-0.012	0.012
R2	-35.055	59.284	-0.945	-35.065	59.273	-0.918	0.009	0.011	-0.026	0.030
R3	-34.334	75.343	-1.059	-34.342	75.346	-1.040	0.008	-0.002	-0.018	0.020
R4	-33.509	92.745	-1.147	-33.516	92.729	-1.112	0.007	0.016	-0.035	0.039
Scratch 1	-29.598	38.839	-0.640	-29.610	38.847	-0.620	0.011	-0.008	-0.020	0.025
Scratch 2	-25.280	28.446	-0.509	-25.279	28.453	-0.488	-0.001	-0.007	-0.021	0.022
Scratch 3	-23.214	23.352	-0.447	-23.215	23.358	-0.432	0.001	-0.006	-0.015	0.016
Shirt	-27.416	8.006	-0.363	-27.420	8.007	-0.362	0.004	-0.001	-0.001	0.004
Shoe	-33.684	18.826	-0.492	-33.683	18.832	-0.488	0.000	-0.007	-0.005	0.008
Stop Sign	-44.683	70.013	-1.099	-44.697	69.994	-1.074	0.014	0.019	-0.025	0.035
Transfer N	-31.715	24.633	-0.534	-31.713	24.647	-0.523	-0.001	-0.014	-0.011	0.018
Transfer S	-27.567	16.471	-0.423	-27.560	16.476	-0.406	-0.008	-0.005	-0.017	0.019
					Ave error in feet		0.007	0.002	-0.016	0.022
					Ave error in centimeters		0.206	0.054	-0.496	0.664

Table A4. PhotoModeler (PM) and total station (TS) coordinate point measurement data using a 24-megapixel camera at 20 meters flying height.

DJI S800	PM X	PM Y	PM Z	TS X	TS Y	TS Z	DX	DY	DZ	Ave Error
Bicycle	-19.006	15.052	-0.293	-19.012	15.062	-0.304	0.005	-0.010	0.011	0.016
Blood	-23.762	8.740	-0.317	-23.765	8.747	-0.336	0.002	-0.007	0.019	0.020
Cellphone	-23.436	34.520	-0.489	-23.440	34.522	-0.521	0.004	-0.003	0.031	0.032
Glove	-22.097	15.577	-0.333	-22.106	15.585	-0.342	0.009	-0.008	0.009	0.015
Hair Tie	-31.661	55.254	-0.762	-31.662	55.246	-0.802	0.002	0.007	0.039	0.040
Helmet	-19.431	8.365	-0.260	-19.437	8.372	-0.259	0.006	-0.007	-0.001	0.009
Hydrant	17.027	63.617	0.959	17.011	63.607	0.934	0.017	0.010	0.024	0.031
Jeans	-27.697	13.264	-0.384	-27.706	13.257	-0.403	0.009	0.007	0.019	0.022
Knife	-28.551	24.548	-0.459	-28.561	24.557	-0.489	0.010	-0.009	0.030	0.033
L1	-30.743	47.467	-0.710	-30.761	47.442	-0.712	0.018	0.025	0.002	0.031
L2	-30.101	59.111	-0.792	-30.118	59.102	-0.821	0.017	0.009	0.029	0.035
L3	-29.366	75.085	-0.917	-29.391	75.066	-0.935	0.024	0.019	0.018	0.036
L4	-28.959	85.047	-0.979	-28.984	85.027	-0.988	0.026	0.021	0.009	0.034
Pen	-35.012	25.654	-0.534	-35.025	25.665	-0.568	0.013	-0.011	0.034	0.038
Plastic	-29.716	36.498	-0.570	-29.730	36.501	-0.601	0.014	-0.003	0.031	0.034
R1	-35.689	47.735	-0.792	-35.693	47.732	-0.808	0.004	0.003	0.016	0.017
R2	-35.054	59.287	-0.902	-35.065	59.273	-0.918	0.011	0.014	0.017	0.024
R3	-34.333	75.347	-1.013	-34.342	75.346	-1.040	0.009	0.001	0.027	0.029
R4	-33.505	92.752	-1.105	-33.516	92.729	-1.112	0.011	0.023	0.008	0.027
Scratch 1	-29.590	38.835	-0.597	-29.610	38.847	-0.620	0.019	-0.012	0.022	0.032
Scratch 2	-25.274	28.443	-0.464	-25.279	28.453	-0.488	0.005	-0.010	0.024	0.027
Scratch 3	-23.209	23.350	-0.395	-23.215	23.358	-0.432	0.006	-0.008	0.037	0.038
Shirt	-27.413	8.004	-0.357	-27.420	8.007	-0.362	0.007	-0.003	0.005	0.009
Shoe	-33.679	18.827	-0.459	-33.683	18.832	-0.488	0.004	-0.005	0.029	0.029
Stop Sign	-44.679	70.018	-1.059	-44.697	69.994	-1.074	0.017	0.024	0.014	0.033
Transfer N	-31.708	24.632	-0.497	-31.713	24.647	-0.523	0.006	-0.015	0.026	0.030
Transfer S	-27.562	16.467	-0.399	-27.560	16.476	-0.406	-0.002	-0.009	0.007	0.011
					Ave error in feet		0.010	0.002	0.020	0.027
					Ave error in centimeters		0.307	0.047	0.604	0.827

APPENDIX B: MOCK ACCIDENT SCENE DIAGRAMS

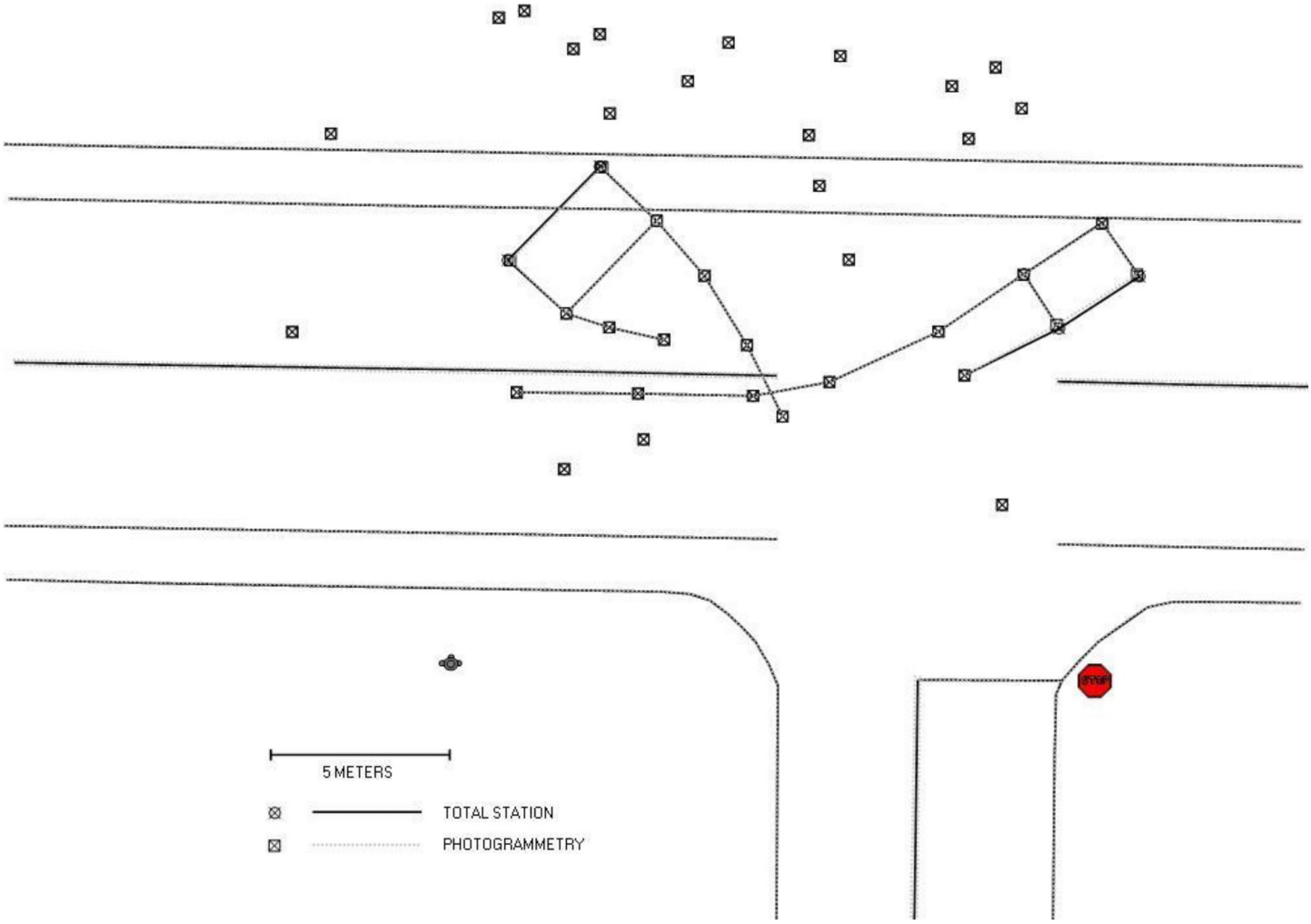

Figure B1. Two vehicle mock accident scene diagram with total station measurement and PhotoModeler measurement overlay. Photogrammetric measurements from aerial images taken by a 4-megapixel integrated camera (Aeryon Scout). No circular targets were used to mark vehicle rest locations.

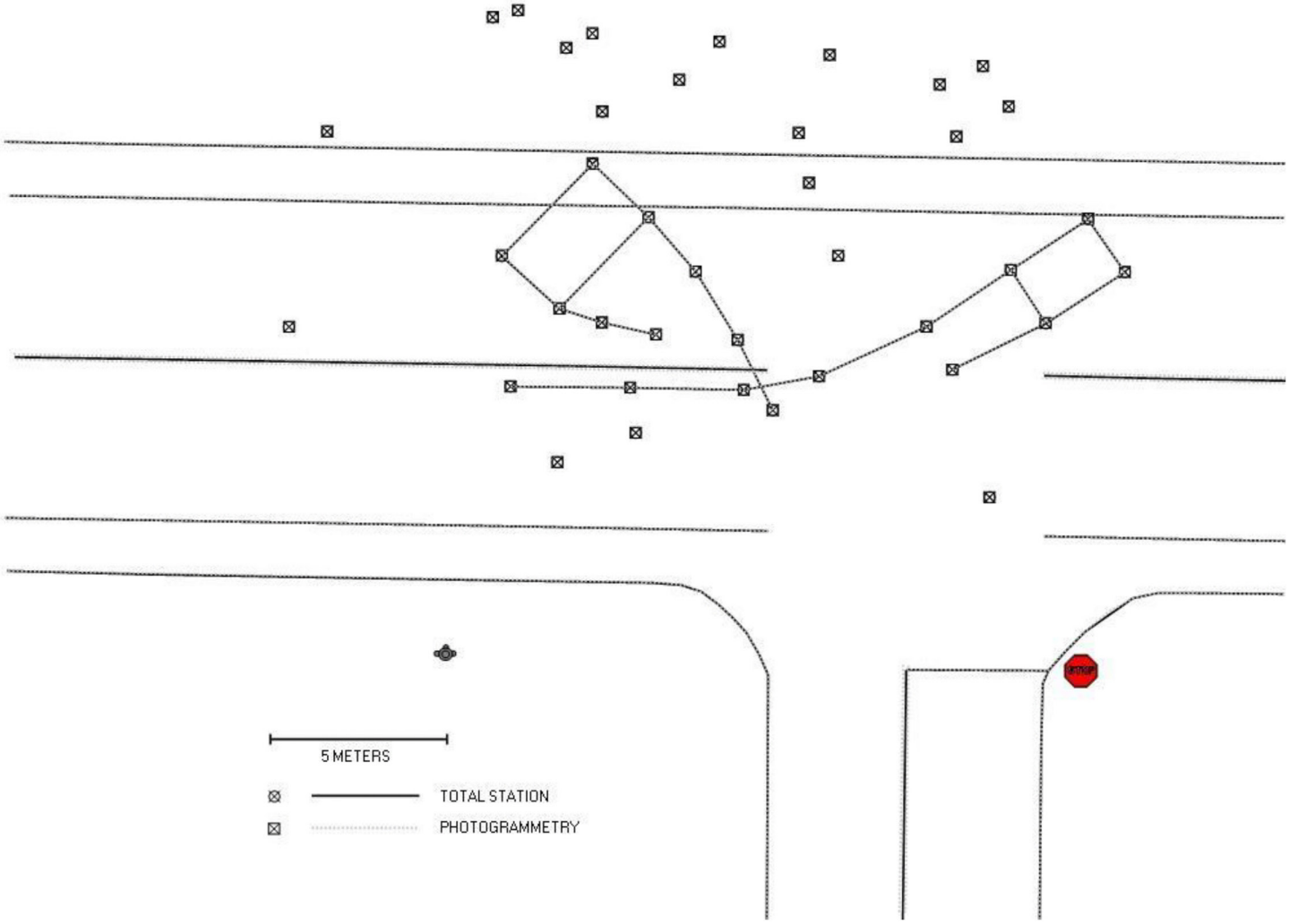

Figure B2. Two vehicle mock accident scene diagram with total station measurement and PhotoModeler measurement overlay. Photogrammetric measurements from aerial images taken by a 24-megapixel consumer grade camera (DJI S800). Circular targets were used to mark vehicle rest locations.

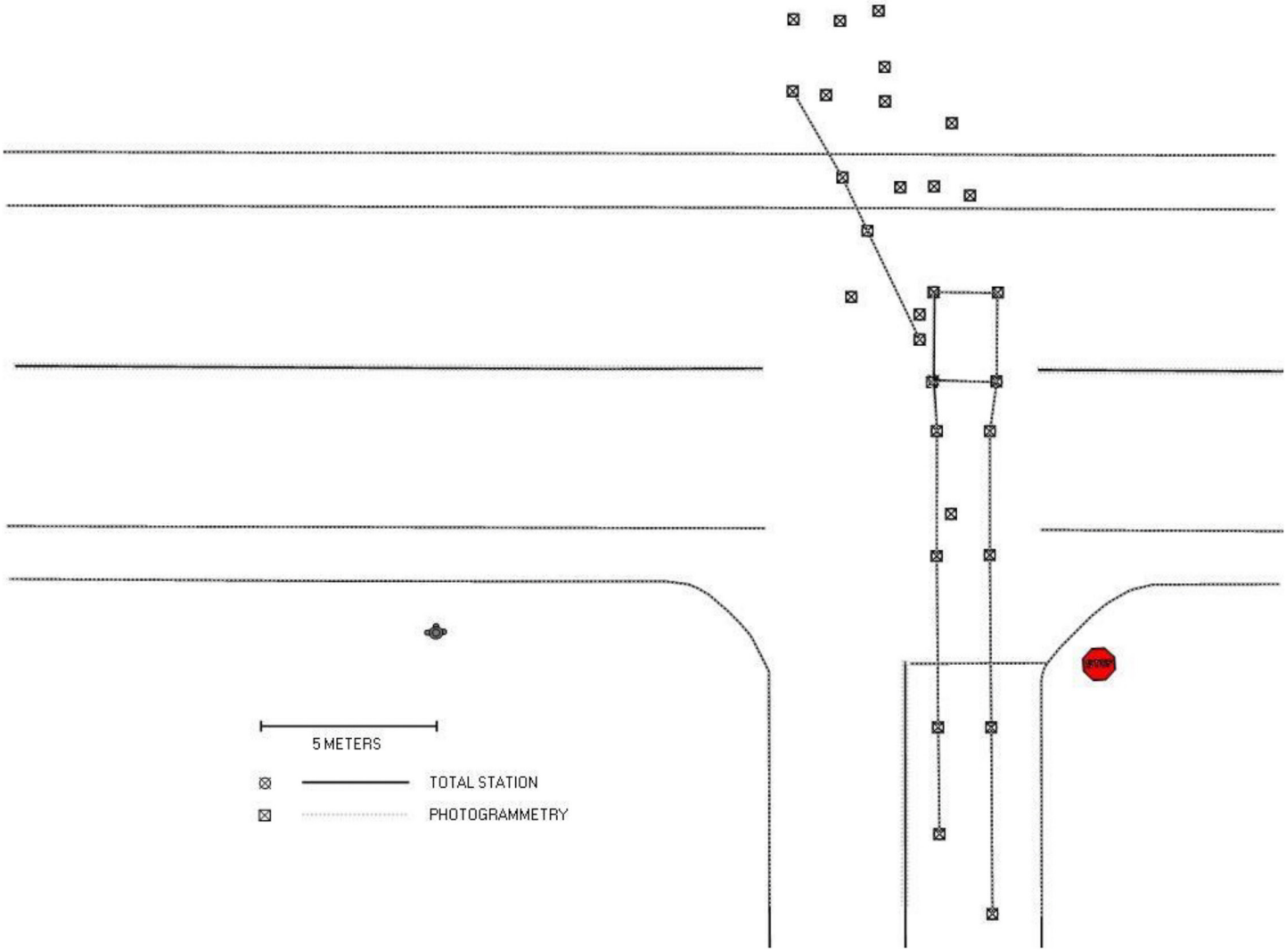

Figure B3. Car versus bicycle mock accident scene diagram with total station measurement and PhotoModeler measurement overlay. Photogrammetric measurements from aerial images taken by a 4-megapixel integrated camera (Aeryon Scout). Circular targets were used to mark vehicle rest locations.

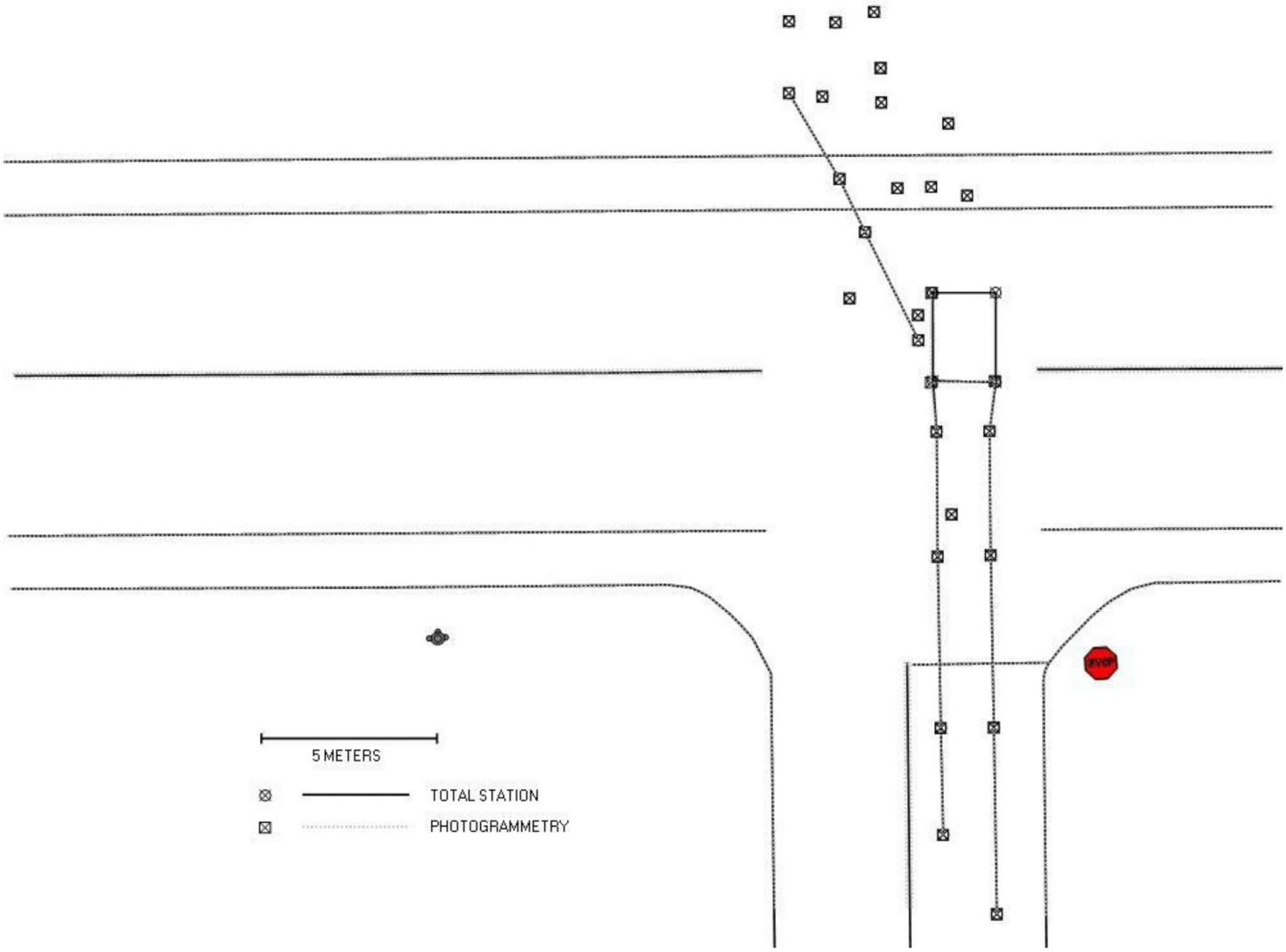

Figure B4. Two car mock accident scene diagram with total station measurement and PhotoModeler measurement overlay. Photogrammetric measurements from aerial images taken by a 24-megapixel consumer grade camera (DJI S800). Circular targets were used to mark vehicle rest locations. No photogrammetry measurement for right front wheel at rest.

APPENDIX C: MOCK ACCIDENT SCENE ORTHOPHOTOS

Figure C1. Two vehicle mock accident scene orthophoto from aerial images taken by a 4-megapixel integrated camera (Aeryon Scout).

Figure C2. Two vehicle mock accident orthophoto from aerial images taken by a 24-megapixel consumer grade camera (DJI S800).

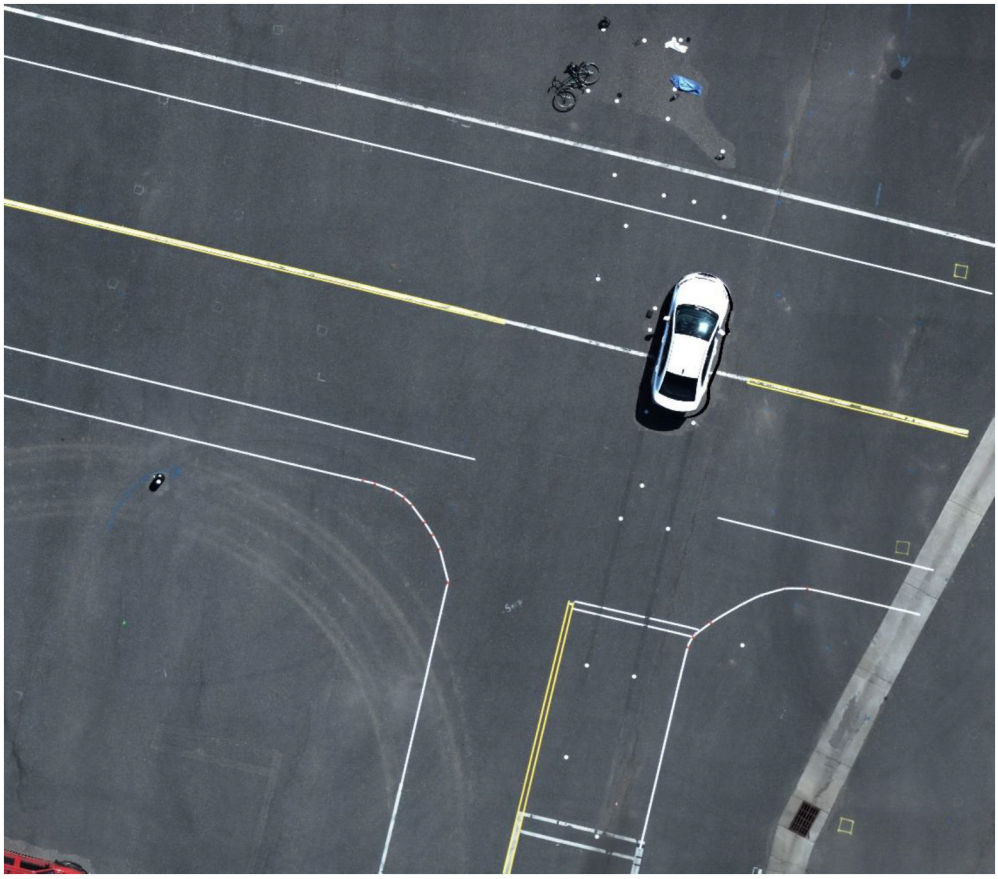

Figure C3. Car versus bicycle mock accident scene orthophoto from aerial images taken by a 4-megapixel integrated camera (Aeryon Scout).

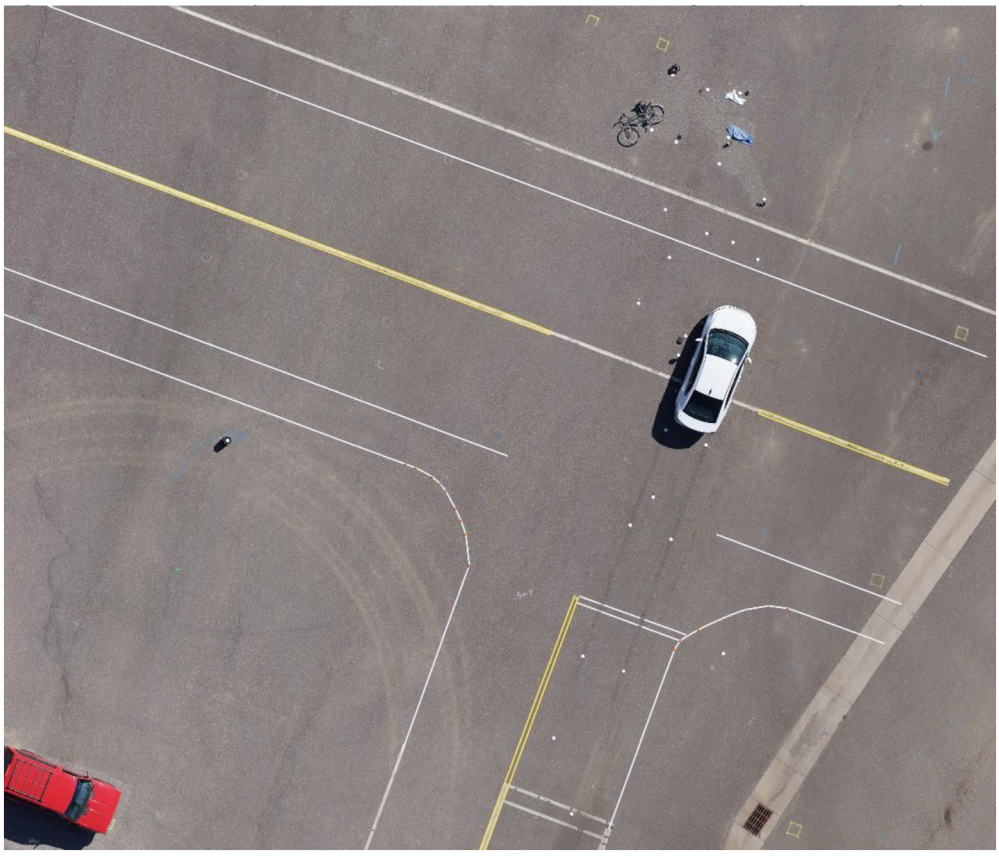

Figure C4. Car versus bicycle mock accident orthophoto from aerial images taken by a 24-megapixel consumer grade camera (DJI S800).